Proceedings of ITC18,2008

ICRF heating in helical reactor

K. Saito, T. Seki, R. Kumazawa, H. Kasahara, T. Mutoh, F. Shimpo, G. Nomura

National Institute for Fusion Science,322-6 Oroshi-cho, Toki 509-5292, Japan

ICRF heating is a favorable high-density plasma heating method since ICRF wave can propagate in high-density plasma. ICRF heating in helical reactor was calculated by using an antenna code and a ray tracing code assuming high-density plasma without resonance layers of α-particles in plasma core. Enough loading resistance and low electric field inside the ICRF antenna was obtained. The strong heating of plasma will be expected in high-density plasma by heating electron and tritium, especially with the configuration of the second harmonic resonance layer of tritium on the magnetic axis shifted onto the saddle point.

Keywords: ICRF heating, helical reactor, LHD, α-particles, ray tracing, ELD/TTMP, second harmonic heating

1. Introduction

Helical fusion reactor [1, 2] has an advantage of steady-state operation since no need for a current drive. Before the ignition in the helical reactor, plasma must be heated by external heating such as ion cyclotron range of frequencies (ICRF) heating, electron cyclotron heating (ECH) and neutral beam injection (NBI). ICRF heating is a favorable high-density plasma heating method since the fast wave launched from ICRF antenna can be transmitted to plasma core even in high-density plasma. In Large Helical Device (LHD) [3], ions were efficiently heated by minority ion heating (hydrogen as minority ions, helium as majority ions) especially by locating ion cyclotron resonance layer on the saddle point of magnetic field strength where the gradient of magnetic field strength is zero, which is characteristic of helical device [4]. Injected energy of 1.6 GJ was achieved mainly using this heating method [5]. Mode conversion heating is also efficient heating method though heating deposition is far off-axis around normalized minor radius of 0.75 [4]. However, there are problems in the ICRF heating in reactor. One is that the loss of fusion-produced α-particles induced by the RF wave [6]. The other is existence of evanescence of the fast wave in vacuum region between plasma and ICRF antennas.

In section 2, resonance configurations to reduce the induced loss of α-particles will be shown. In section 3, calculation of loading resistance and electric field in the ICRF antenna will be shown. Ray tracing analysis will be conducted in section 4. Section 5 is a summary section.

2. Candidate of frequency and magnetic field strength in helical reactor

It was shown by the Monte Carlo simulation that α-particles are well confined without RF field [7]. We propose the configurations where the second harmonic resonance layer of tritium locates at the plasma core and the resonance layers of α-particles locate out of the plasma core to reduce the induced loss of α-particles by RF waves. Figure 1-a shows the ion cyclotron resonance layers at the vertically elongated toroidal section, where $f = n f_{ci}$. Magnetic configuration is the same with that of LHD (R_{ax}=3.75 m, vacuum), except for the scale factor of 3.5. The magnetic field strength on axis B_{ax} is 4.92 T and the RF frequency f is 50 MHz. The second harmonic resonance layers of α-particles do not exist inside of last closed flux surface and only the fundamental resonance layer locates in high-field peripheral region of the plasma. Therefore, loss of high-energy α-particles by RF field is expected to reduce and the energy of α-particles will be sufficiently utilized for plasma heating and the heat load by the α-particles on divertor plates or first wall will be kept low. A second harmonic resonance layer of tritium locates on the magnetic axis, therefore tritium heating is expected as well as electron heating by electron Landau damping (ELD) / transit-time magnetic pumping (TTMP) heating. Figure 1-b shows the resonance layers in the case of B_{ax}=5.10 T and f=50 MHz. A fundamental α-particle

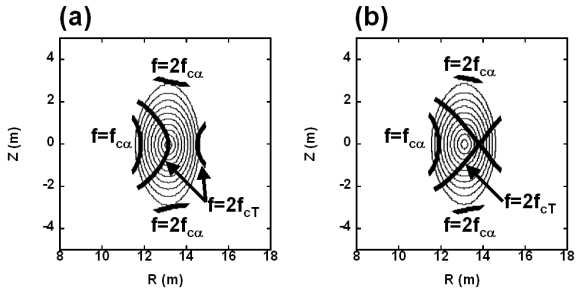

Fig.1 Configurations of ion cyclotron resonance layers. (a) Resonance layer of tritium on magnetic axis (f=50 MHz, B_{ax}=4.92 T). (b) Resonance layer of tritium on saddle point (f=50 MHz, B_{ax}=5.10 T).

author's e-mail: saito@nifs.ac.jp

resonance a little approaches to the plasma core and the resonance layer of tritium does not locate on the magnetic axis, however it locates at the saddle point where the efficient ion heating is expected.

3. Calculation of ICRF antenna performance

The loading resistance and the electro magnetic field around ICRF antenna were calculated by using variational method [8]. In this calculation slab model of plasma was used and infinite area of Faraday shield and back plate was assumed. Wave launched from antenna never returns to antenna. Simplified dielectric tensor of cold plasma was used, where a component of electric field along to magnetic field line is zero. The size of model antenna was 600 mm in strap width, 1000 mm in strap height, 50 mm between Faraday shield and the strap, and 350 mm between the strap and the back-plate. Large distance of 500 mm between plasma and Faraday shield was assumed to avoid the intense heat load on the ICRF antenna. RF frequency was 50 MHz and the magnetic field strength was 4.5 T (constant). Parabolic density profile was assumed with the peak density of 2×10^{20} m^{-3}. Ion species were deuterium and tritium with the same concentration. Power was fed into the two straps of upper and lower antenna by the coaxial lines with the characteristic impedance Z_c of 50 Ω through an outer port at the vertically elongated toroidal section assuming FFHR-2S [2] since it is not necessary to use blanket area for the feed lines. By the calculation, it was found that the loading resistance R was 10 Ω in the case of the opposite current direction on straps. Assuming maximum voltage in the coaxial line V_{max} of 70 kV, which is the twice of the interlock level in LHD, the allowable injection power by two antennas was estimated to be 19.6 MW by using the equation

$$Power = \frac{1}{2} R \left(\frac{V_{\max}}{Z_c} \right)^2 . \qquad (1)$$

Electric field inside the antenna was also calculated. The strength of electric field between Faraday shield and strap was the largest. In the case of 19.6 MW injection, it was 8.1 kV/cm and was smaller than that of breakdown for E⊥B (>30 kV/cm) [9]. Figure 2-a shows the intensity of the component of pointing vector directed to plasma. Peaks locate near the antenna tips. In the case of the same current direction on straps, loading resistance of 9.5 Ω and the power of 18.6 MW is possible. Maximum electric field was 14.2 kV/cm and still allowable level. The peak of intensity of pointing vector located between antennas as shown in Fig. 2-b.

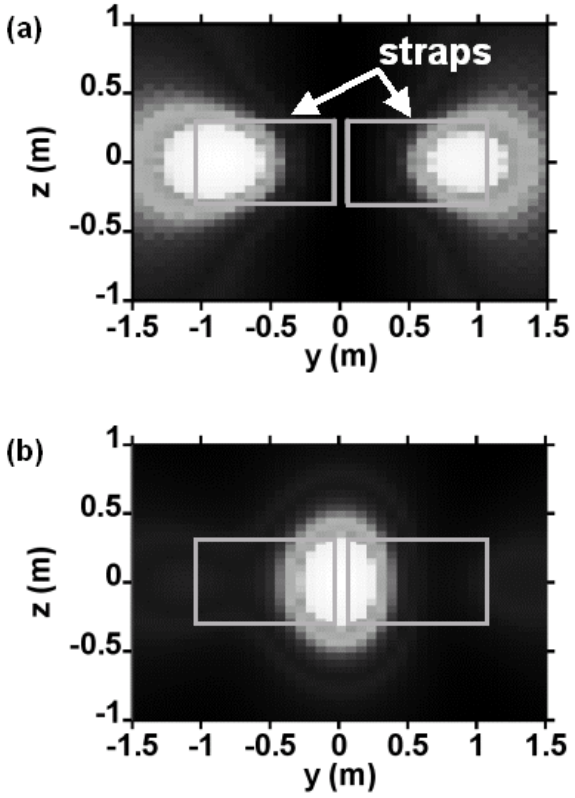

Fig.2 Intensity of the component of pointing vector directed to plasma at the plasma edge. (a) Opposite current direction case. (b) Same current direction case.

4. Ray-tracing calculation of ICRF wave in helical reactor

The ray tracing calculation was conducted using the peaks of pointing vector obtained in section 3 as initial positions. Four combinations of initial wave number parallel to magnetic field line and the wave number perpendicular to the magnetic field line projected on the flux surface of $(k_{//}, k_{\perp})$ =(-0.7 m^{-1}, -0.7 m^{-1}), (-0.7 m^{-1}, 0.7 m^{-1}), (0.7 m^{-1}, -0.7 m^{-1}), (0.7 m^{-1}, 0.7 m^{-1}) were supposed since waves are evanescent for larger wave numbers. In this calculation, magnetic field configuration of LHD was used with the scale factor of 3.5. Dielectric tensor of cold plasma was used for the calculation of ray trajectory and polarization. Absorbed power was calculated by using the absorption ratio Q and the wave energy W,

$$Q = \frac{\varepsilon_0}{2} \omega \vec{E}^* \cdot \vec{K}^a \cdot \vec{E} \qquad (2)$$

$$W = \frac{1}{4\mu_0} \vec{B}^* \cdot \vec{B} + \frac{\varepsilon_0}{4} \vec{E}^* \cdot \frac{\partial \omega \vec{K}^h}{\partial \omega} \cdot \vec{E} \qquad (3)$$

where, $\vec{E}$ is the polarized electric field and $\vec{K}$ is the hot plasma dielectric tensor. The absorbed power was superposed with the same weight ignoring the effect of interference. High density plasma with internal diffusion barrier (IDB) [10] with the following profiles of electron density and temperatures of ions and electrons were supposed,

$$n_e = n_{e0}[0.8\exp\{-(\rho/0.35)^{2.5}\} + 0.1(1-\rho^{6.5}) + 0.1] \quad (4)$$

$$T_{i,e} = T_{i,e0}(1-\rho^4) \quad (5)$$

where, ρ is the normalized minor radius. Deuterium and tritium was the same concentration, and the fusion products and the impurities were ignored. Ion and electron temperatures on magnetic axis $T_{i,e0}$ were 8 keV. The electron density on magnetic axis n_{e0} was scanned from 1×10^{20} m^{-3} to 5×10^{20} m^{-3} supposing high-density ignition.

4-1 Opposite current direction on straps

Ray tracing calculation was conducted from two initial positions where the strength of pointing vector shown in Fig 2-a is the maximum in the case of the opposite current direction on straps. The resonance layer of tritium located on the magnetic axis as shown in Fig 1-a. Figure 3-a shows variation of $k_{//}$. In spite of the small initial $k_{//}$, it was strongly enlarged, especially with the high electron density. The large $k_{//}$ up-shift is the characteristic to helical devices as pointed out in ref. [11]. These large $k_{//}$ is preferable for the direct electron heating by ELD and/or TTMP since the components for electron heating of $\vec{K}^a$ (anti-Hermitian part of $\vec{K}$) are proportional to $\exp\{-(\omega/k_{//}v_{te})^2\}$. In Fig. 3-b, the values of $\exp\{-(\omega/k_{//}v_{te})^2\}$ for different electron densities were shown, and they grew up enough close to one.

Figure 4-1-a shows the integrated absorbed energy by electron and tritium. Absorption increased with the plasma density, and the portion of absorption by electron and tritium was changed. Wave energy was absorbed mainly by tritium at low density, whereas, wave energy was absorbed mainly by electron at high density since before cyclotron resonance of tritium, electrons start to absorb wave energy due to enhanced electron heating at high density. Figure 4-1-b shows power deposition profile. Location of power deposition is near plasma but a little off-axis (ρ≈0.25). Figure 4-2-a shows the absorbed energies in the case of resonance on the saddle point. In this case, the ratio of tritium heating increased since rays experienced the resonance of tritium earlier. Therefore, deposition profile shifted outward as shown in Fig. 4-2-b.

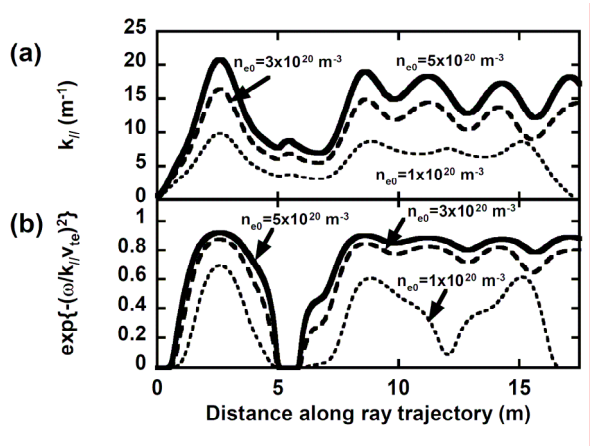

Fig.3 (a) Variation of $k_{//}$ for three electron densities on magnetic axis. (b) Variation of $\exp\{-(\omega/k_{//}v_{te})^2\}$ as an index of ELD/TTMP strength.

4-2 Same current direction on straps

Initial position was set at the outer edge on mid-plane at the perpendicularly elongated plasma section, since the pointing vector was maximum there in the case of the same current direction on straps as shown in Fig 2-b. Ray tracing was conducted for two cases of resonance of tritium on the magnetic axis and the saddle point. As shown in Fig.4-3-a, in the case of resonance on the axis, tritium heating was dominant and power was deposited on the magnetic axis (Fig.4-3-b). One-pass absorption was small when the density was low. However, by the configuration of resonance layer of tritium on saddle point, it increased though the peak of deposition shifted around ρ=0.5 as shown in Figs. 4-4-a and 4-4-b. Therefore the configuration of the magnetic axis on the saddle point may be useful for intense core heating. The magnetic axis was shifted onto the saddle point artificially and resonance layer of tritium was located on the axis. In this case, the intense core heating by tritium was calculated as shown in Figs. 4-5-a and 4-5-b. The second harmonic heating was thought to be enhanced by the effects of large $k_{\perp}$ around the axis and low gradient at the saddle point. Due to the strong absorption by tritium, electrons were not heated. Since the wave energy is dumped at the magnetic axis perfectly before the growing up of $k_{//}$, even if resonance of α-particles exists in plasma by the Doppler effect, the acceleration of α-particles will be avoided.

5. Summary

To reduce the enhanced loss of α-particles by RF waves, the configurations without the cyclotron

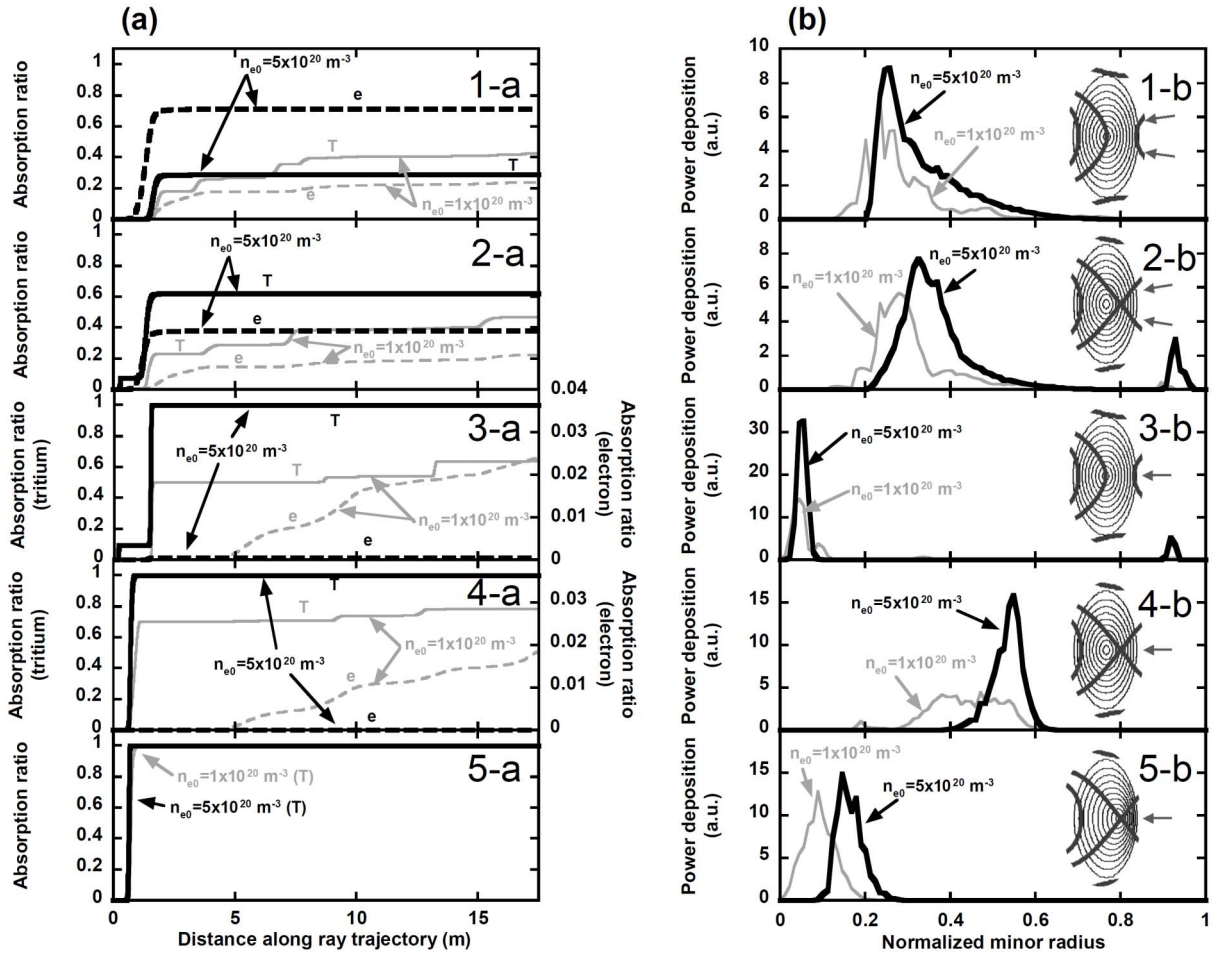

Fig.4 (a) Absorbed wave energy by electron and tritium normalized by initial wave energy for various initial positions and resonance configurations. (b) Deposited power density multiplied by dV/dρ. At the right side, initial positions and resonance configurations are shown.

resonance of α-particles layer in plasma core were selected as candidates for ICRF heating in helical reactor. The second harmonic resonance layer of tritium located at the plasma core. ICRF antenna for the helical reactor was not optimized but the large loading resistance of 10 Ω and the power injection of 20 MW from two antennas were found to be achievable. By the calculation of ray tracing, it was found that the wave number parallel to magnetic field was up-shifted largely especially in high-density IDB plasma even if the initial wave number was small, which enabled ELD/TTMP heating. The configuration of the second harmonic resonance layer on the magnetic axis shifted onto the saddle point makes the intense core heating possible by emitting the RF wave from mid plane.

References

[1] A. Sagara, et al.,Fusion Eng. Des. 83 (2008) 1690-1695.

[2] N. Yanagai, K. Nishimura, A. Sagara, Design of Split-Type Helical Coils for FFHR-2S, NIFS Annual Report, 2006-2007, p.269.

[3] O. Motojima, et al., Nucl. Fusion 47 (2007) S668-S676.

[4] K. Saito, R. Kumazawa, T. Mutoh, T. Seki, T. Watari, Y. Torii, et al., Nucl. Fusion 41 (2001) 1021-1035.

[5] K. Saito, et al., J. Nucl. Mater. 363-365 (2007) 1323-1328.

[6] D. S. Darrow, et al., PPPL Reports, PPPL-3164 (1996).

[7] S. Murakami, H. Yamada, M. Sasao, M. Isobe, T. Ozaki, T. Saida, et al., Fusion Sci. Technol. 46 (2004) 241-247.

[8] K. Theilhaber, J. Jacquinot, Nucl. Fusion 24 (1984) 541-554.

[9] S.J. Wukitch, et al., 2002 proc .19th Int. Conf. on Fusion Energy 2002 (Lyon, France, 2002) (Vienna: IAEA) CD-ROM file FT/P1-14 and http://www.iaea.org/programmes/ripc/physics/fec2002/html/fec2002.htm.

[10] N. Ohyabu, et al., Plasma Phys. Control. Fusion 48 (2006) B383-B390.

[11] N. Takeuchi, et al., J. Plasma Fusion Res. SERIES, Vol.6 (2004) 642-646.